

# Correlation between structural, magnetic and spectroscopic properties of Mg substituted $\text{CoFe}_2\text{O}_4$

GNANA PRAVEENA NETHALA<sup>1,\*</sup>, RAVINDAR TADI<sup>2</sup>, AROLI VENKATESWARA ANUPAMA<sup>3</sup>,  
SATISH LAXMAN SHINDE<sup>3</sup>, V. VEERAIAH<sup>1</sup>

<sup>1</sup>Department of Physics, Andhra University, Visakhapatnam-530003, India

<sup>2</sup>Korea Research Institute of Standards and Science, Daejeon 305-340, Korea

<sup>3</sup>Indian Institute of Science, Bangalore-560012, India

Mg substituted cobalt ferrite spinel powder samples with the general formula  $\text{Mg}_x\text{Co}_{1-x}\text{Fe}_2\text{O}_4$  ( $x = 0$  to 0.25) were synthesized chemically through sol-gel method and annealed at 1100 °C for 2 h. They were initially screened for the structural and morphological properties by X-ray diffraction and field emission scanning electron microscopy, respectively. Vibrational properties of the samples were studied by Raman and infrared spectroscopies. X-ray diffraction confirmed the formation of single pure or near-pure phase with cubic spinel structure for all the samples with expected occupancy values. The field emission scanning electron microscopy revealed a decrease in the particle size with an increase in Mg concentration. Both structural and magnetic properties of the samples were characterized using Mössbauer spectroscopy while the magnetic properties were studied using vibrating sample magnetometry. The changes in magnetic moment of ions, their coupling with neighboring ions and cation exchange interactions were confirmed from the Mössbauer spectroscopy analysis. Saturation magnetization and coercivity values can be explained based on the Slater-Pauling curve. The magnetometry results showed a decrease in saturation magnetization of the samples with increase in Mg concentration.

Keywords: *Mg substituted cobalt ferrite; sol-gel method; Rietveld refinement; vibrational properties; spectroscopic techniques*

## 1. Introduction

Cubic spinel ferrites exhibit excellent magnetic and electrical properties suitable for data storage devices, magnetic sensors, actuators, targeted drug delivery and medical diagnosis applications [1–4]. In addition to the high electrical resistivity and good magnetic properties, ferrites are used as an excellent core material for power transformers in electronics and telecommunications [5, 6].  $\text{CoFe}_2\text{O}_4$ , a member of this spinel family, has unique magnetic properties with high coercivity, moderate saturation magnetization, large magnetic anisotropy, high chemical stability, wear resistance and electric insulation [7–10].

Spinel ferrites can be generally categorized into three types based on the occupancies of cations at the tetrahedral (Th- or A-) and octahedral (Oh- or B-) interstitial sites as normal, inverse and mixed

spins. The normal spinel has all the divalent (A) cations on the tetrahedral (Th-) sites and the trivalent (B) cations on the octahedral (Oh-) sites which can be represented as  $(\text{A})_{\text{tet}}[\text{B}_2]_{\text{oct}}\text{O}_4$ . The inverse spinel, has the divalent cations occupying (Oh-) sites and trivalent cations are divided among the Th- and remaining Oh-sites which can be represented as  $(\text{B})_{\text{tet}}[\text{AB}]_{\text{oct}}\text{O}_4$ . The third category is mixed spinel with cation distribution denoted by  $(\text{A}_x\text{B}_{1-x})_{\text{tet}}[\text{A}_{1-x}\text{B}_{1+x}]_{\text{oct}}\text{O}_4$  with an interchange of cations among the tetrahedral and octahedral occupancies with a possibility to control the properties by selecting a substituent and an appropriate synthesis method. Several methods, such as co-precipitation, thermal decomposition, sol-gel and microemulsion, have been employed for the synthesis of  $\text{CoFe}_2\text{O}_4$  powders with controlled properties (via cation occupancies) depending on the method of preparation [11–18].

The properties of this ferrite can be tuned via substitution by non-magnetic cations (such as

\*E-mail: praveenajoy777@gmail.com

$\text{Mg}^{2+}$ ) and it was observed that  $\text{Mg}^{2+}$  ions occupy B-sites due to their strong tendency towards B-sites [19, 20]. The number of intersite cations exchanged between tetrahedral and octahedral sites is equivalent leading to disorder in the long range ordering [21]. The magnetic behavior of  $\text{CoFe}_2\text{O}_4$  is due to the super exchange interaction between the distributed cations and bond lengths [22, 23]. The bond length at A-site is abnormally long compared to B-site [24]. Substitution of Mg in cobalt site can lead to three possible co-ordinations such as: with A- or B- or AB-sites mediated by oxygen ions [25–27]. In the present study, we have investigated the structural, magnetic and spectroscopic properties of Mg- substituted  $\text{CoFe}_2\text{O}_4$  prepared by sol-gel method.

## 2. Experimental

Mg-substituted  $\text{CoFe}_2\text{O}_4$  [ $\text{Co}_{1-x}\text{Mg}_x\text{Fe}_2\text{O}_4$  ( $x = 0.05$  to  $0.25$ )] were prepared by sol-gel method using  $\text{Co}(\text{NO}_3)_3 \cdot 6\text{H}_2\text{O}$ ,  $\text{Fe}(\text{NO}_3)_3 \cdot 9\text{H}_2\text{O}$  and  $\text{Mg}(\text{NO}_3)_2 \cdot 6\text{H}_2\text{O}$  as metal nitrate precursors and citric acid ( $\text{C}_6\text{H}_8\text{O}_7 \cdot \text{H}_2\text{O}$ ) as chelating agent. The stoichiometric amounts of the starting materials were dissolved in 10 mL of methanol in a borosil beaker. The beaker was kept on a hot plate maintained at  $80^\circ\text{C}$  and the content was mixed thoroughly using a magnetic stirrer till gel formation. The process of heating at  $80^\circ\text{C}$ , while stirring was continued which finally resulted in dark reddish brown gel formation after heating for  $\sim 3$  h to 4 h, resulting in the conversion of the gel to ash powder. The powder was calcined at  $450^\circ\text{C}$  for  $\sim 1$  h to remove the volatile components. The samples were ground and annealed at  $1100^\circ\text{C}$  at a rate of  $5^\circ\text{C}$  per minute for 2 h in order to obtain the final product.

Crystal structure of the synthesized samples was studied by X-ray diffraction (PANalytical,  $\text{CuK}\alpha$  ( $\lambda = 1.54056\text{\AA}$ )). The diffraction data were collected in the detector angle  $2\theta$  range of  $10^\circ$  to  $90^\circ$  with a step size of  $0.0263^\circ$ . The crystalline phases in the samples were identified by generating simulated patterns using crystallographic information files (CIF) from inorganic crystal

structure database (ICSD) and matching to experimental XRD data. Rietveld refinement [28] of the XRD data was carried out using the program FullProf [29] to extract structural and compositional details as well as the phase partitioning of constituents in the sample. During the refinement, instrumental error corrections were considered. For the refinement, Thomson-Cox-Hastings profile was adopted. The lattice parameters, scale factor, full width at half maximum (FWHM) of the Bragg reflections from the phases were refined. The quality of the fit to the observed XRD patterns were assessed by the Rietveld agreement factors: R-pattern factor ( $R_p$ ), R-weighted pattern factor ( $R_{wp}$ ), R-expected ( $R_{exp}$ ) and  $\chi^2$  [28]. The quality of the fit was good with  $\chi^2$  between  $\sim 1$  and 2.5. The refined lattice parameters and occupancy factors of cations in the cubic spinel interstitials were obtained. The crystallite sizes were estimated using Scherrer method [30]. The Rietveld refined XRD patterns are shown in Fig. 2 and the results after refinement are tabulated in Table 1.

Field emission scanning electron microscope (FE-SEM, Germany) was used to study the surface morphology. The coercivity and the saturation magnetization were determined by a vibrating sample magnetometer (Lakeshore, USA).

$^{57}\text{Fe}$  Mössbauer spectroscopy (SEECO, USA) was used to study the local magnetic ordering and magnetic behavior. All the synthesized samples (i.e.  $x = 0, 0.05, 0.1, 0.15, 0.2$  and  $0.25$ ) were characterized by  $^{57}\text{Fe}$  Mössbauer spectroscopy in transmission mode. The spectra were recorded by using a gas proportional counter. The velocity of Mössbauer drive was calibrated using  $\alpha$ -Fe foil at RT. The spectra obtained were least square fit using “NORMOS” program [44, 45]. The Mössbauer lines were fit with Lorentzian profile. The spectra after the least square fit are shown in Fig. 7. The Mössbauer spectral parameters such as isomer shift (IS), quadrupole splitting (QS), magnetic hyperfine field ( $B_{hf}$ ) and spectral area were obtained and tabulated in Table 4. All the isomer shifts were given with respect to the  $^{57}\text{Co}$ -source (Rh-matrix) that produces an isomer shift of  $-0.106\text{ mm/s}$  relative to the source.

The qualitative phase analysis of the samples was done by FT-IR spectroscopy (PerkinElmer, USA). Raman spectroscopy (WiTec, Japan) was used to characterize the lattice distortion, local cation distribution and vibrational modes of the spinel structure.

### 3. Results and discussion

#### 3.1. X-ray diffraction XRD and Rietveld refinement

All the samples showed the formation of cubic spinel ferrite (for intended phase) with Fd-3m structure (Fig. 2). The pristine  $\text{CoFe}_2\text{O}_4$  is a cubic mixed spinel with lattice parameter typical of nanosized sample [31]. With  $\text{Mg}^{2+}$  substitution, the lattice parameter showed a very slight decreasing trend in value. This has been expected as  $\text{Mg}^{2+}$  has ionic radii 0.57 Å in tetrahedral coordination which substitutes for the only slightly bigger  $\text{Co}^{2+}$  ion in A-site (0.58 Å) [32, 33] at moderate dopant concentration (up to  $x = 0.25$ ). However, there exists a discrepancy in lattice parameter variation with substituent concentration in our samples as the synthesis conditions and post-synthesis annealing temperatures could be slightly different. Also, a few samples (Table 1) showed the formation of a small amount of impurity phase, like in samples  $x = 0.15$  and  $x = 0.2$ . However, in the case of sample  $x = 0.15$ , there was no obvious impurity phase; a close inspection showed the formation of another cubic spinel phase in addition to the intended phase  $\text{Co}_{0.85}\text{Mg}_{0.15}\text{Fe}_2\text{O}_4$ , which agreed with the lattice parameters of  $\text{CoFe}_2\text{O}_4$  [34]. The amount of  $\text{CoFe}_2\text{O}_4$  phase was estimated to be in a similar proportion to that of the intended doped phase. The sample  $x = 0.2$  showed the trace presence of hematite phase (~1.8 wt.%). As this impurity phase formation is not consistent with substituent concentration, the observed deviation can be attributed to the possible variation in synthesis or post synthesis heat treatment conditions of the said samples. The crystallite sizes were estimated by Scherrer formula from the (3 1 1) peak in the case of spinel ferrite phase while for hematite phase, the most intense (1 0 4) Bragg reflection was

chosen. The peak widths were obtained from Rietveld refinement results for each phase. The crystallite sizes of all the identified phases are listed in Table 1. The samples are nanosized with crystallite sizes between 30 nm to 85 nm.

In the Rietveld refined XRD plots of samples (Fig. 1), the samples which have  $\text{CoFe}_2\text{O}_4$  phase along with intended substituted spinel ferrite phase are indexed only for the intended phase, since both phases have nearly overlapping Bragg positions.

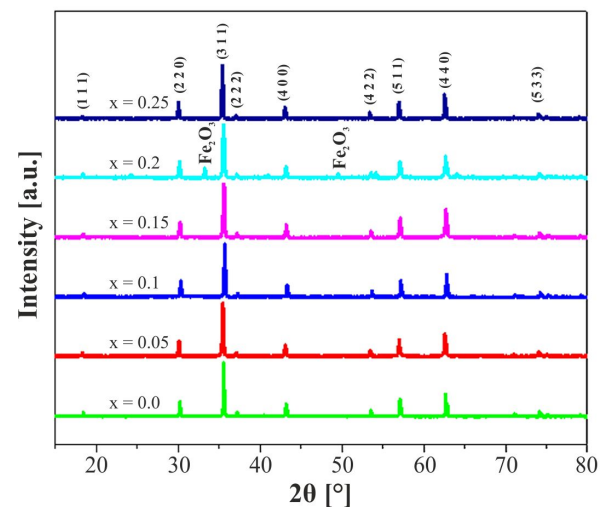


Fig. 1. X-ray diffraction patterns of  $\text{Co}_{1-x}\text{Mg}_x\text{Fe}_2\text{O}_4$  powder samples annealed at 1100 °C for 2 h.

#### 3.2. Field emission scanning electron microscopy (FE-SEM)

FE-SEM micrographs of  $\text{Co}_{1-x}\text{Mg}_x\text{Fe}_2\text{O}_4$  ( $x = 0.05$  to 0.25) samples annealed at 1100 °C for 2 h are shown in the Fig. 3. The particles have an almost homogeneous distribution with agglomerated grains. The shape of the grains is spherical for all the compounds. The particle size of the Mg substituted  $\text{CoFe}_2\text{O}_4$  decreases with an increase in  $\text{Mg}^{2+}$  concentration as evidenced by the FE-SEM images. The atomic ratios of Fe/Co obtained from EDX patterns confirm the stoichiometric sample formation for all the samples. The compositions have an average particle size of ~3 µm to 4 µm. The atomic percentages of cobalt, iron, oxygen and magnesium in the pristine and doped  $\text{CoFe}_2\text{O}_4$  are given in Table 2.

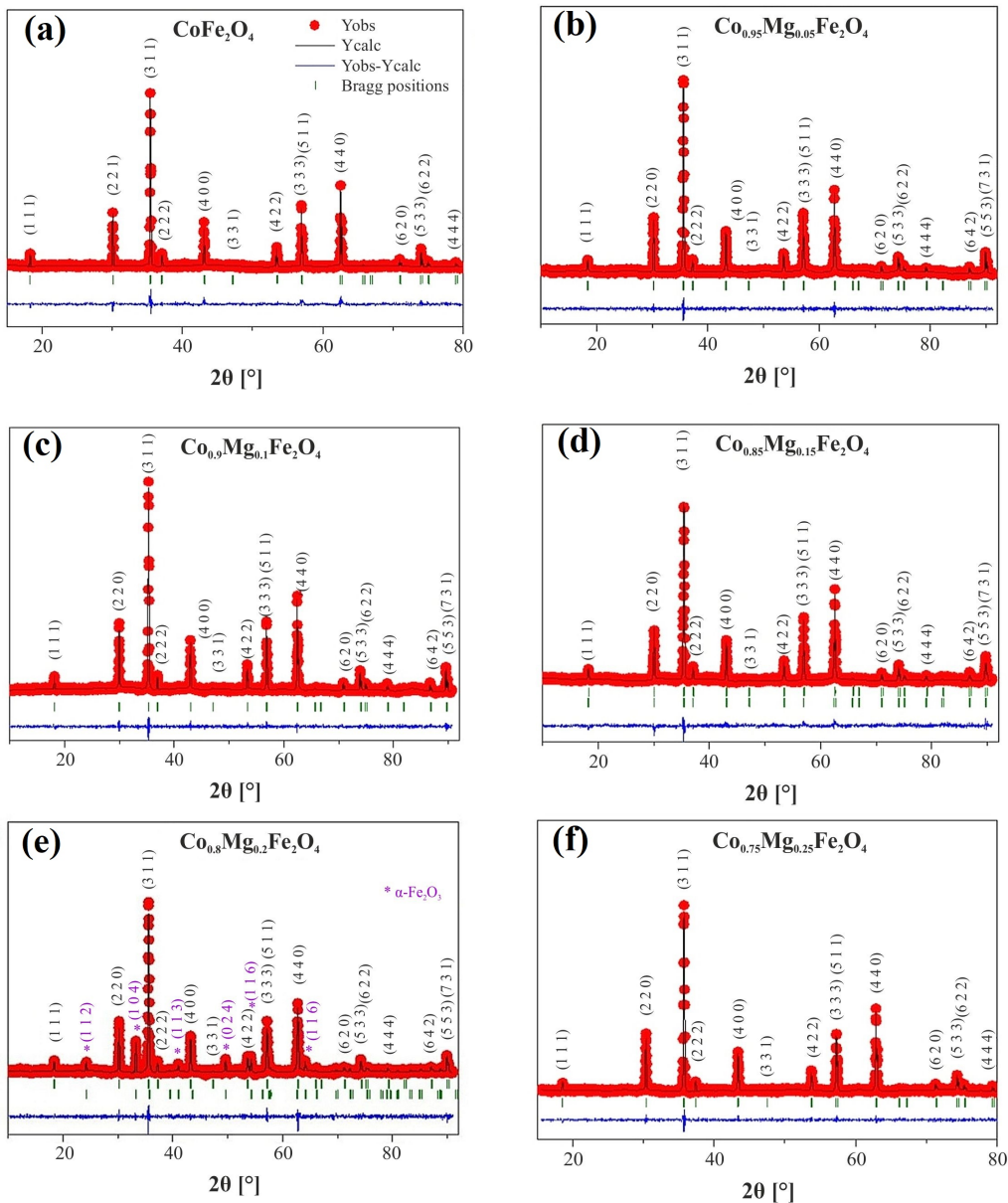


Fig. 2. Rietveld refined XRD patterns of samples annealed at 1100 °C for 2 h: (a)  $x = 0.0$ , (b)  $x = 0.05$ , (c)  $x = 0.1$ , (d)  $x = 0.15$ , (e)  $x = 0.2$  and (f)  $x = 0.25$ . The circles represent experimental data, and the solid lines represent the least square fit by simulation using FullProf program. The lines at the bottom of each fit pattern show the difference between the experimental and refined data. The vertical lines below each fit XRD pattern indicate the Bragg positions.

### 3.3. Fourier transform infrared (FT-IR) spectroscopy

Fig. 4 shows the FT-IR spectra of Mg substituted  $\text{Co}_{1-x}\text{Mg}_x\text{Fe}_2\text{O}_4$  samples annealed at 1100 °C, recorded at room temperature in a wave-

number ranging from  $400 \text{ cm}^{-1}$  to  $4000 \text{ cm}^{-1}$ . FT-IR spectroscopy is a technique used to investigate the structural properties and distribution of cations between octahedral and tetrahedral sites of cubic spinel  $\text{CoFe}_2\text{O}_4$ . The FT-IR spectra of the samples show the presence of two

Table 1. Rietveld refinement results for  $\text{Co}_{1-x}\text{Mg}_x\text{Fe}_2\text{O}_4$  with  $x = 0$ ,  $x = 0.05$ ,  $x = 0.1$ ,  $x = 0.15$ ,  $x = 0.2$ ,  $x = 0.25$ , unit cell volume [ $\text{\AA}^3$ ], crystallite size [nm] and cation distribution.

Sample	Composition	Cell parameter [ $\text{\AA}$ ], unit cell volume [ $\text{\AA}^3$ ]	Crystallite size [nm]	Cation distribution [%]	
				A-site	B-site
1	$\text{CoFe}_2\text{O}_4$	8.3848, 589.5	80.7	$\text{Co}_{0.28}\text{Fe}_{0.74}$	$\text{Co}_{0.70}\text{Fe}_{1.3}$
2	$\text{Co}_{0.95}\text{Mg}_{0.05}\text{Fe}_2\text{O}_4$	8.3805, 588.6	52.2	$\text{Co}_{0.106}\text{Mg}_{0.049}\text{Fe}_{0.85}$	$\text{Co}_{0.85}\text{Mg}_{0.007}\text{Fe}_{1.2}$
3	$\text{Co}_{0.9}\text{Mg}_{0.1}\text{Fe}_2\text{O}_4$	8.3855, 588.8	69.9	$\text{Co}_{0.1}\text{Mg}_{0.10}\text{Fe}_{0.851}$	$\text{Co}_{0.85}\text{Mg}_{0.0004}\text{Fe}_{1.15}$
4	$\text{Co}_{0.85}\text{Mg}_{0.15}\text{Fe}_2\text{O}_4$ $\text{CoFe}_2\text{O}_4$	8.3814, 588.8 8.3916, 590.9	79.3 29.9	$\text{Co}_{0.07}\text{Mg}_{0.14}\text{Fe}_{0.79}$	$\text{Co}_{0.77}\text{Mg}_{0.0046}\text{Fe}_{1.23}$
5	$\text{Co}_{0.8}\text{Mg}_{0.2}\text{Fe}_2\text{O}_4$ $\alpha\text{-Fe}_2\text{O}_3$	8.3725, 586.9 a, b = 5.0298, c = 13.708, V = 300.3	43.5 50.7	$\text{Co}_{0.005}\text{Mg}_{0.197}\text{Fe}_{0.80}$	$\text{Co}_{0.79}\text{Mg}_{0.006}\text{Fe}_{1.2}$
6	$\text{Co}_{0.75}\text{Mg}_{0.25}\text{Fe}_2\text{O}_4$	8.3716, 586.7	61.6	$\text{Co}_{0.1}\text{Mg}_{0.22}\text{Fe}_{0.77}$	$\text{Co}_{0.73}\text{Mg}_{0.0024}\text{Fe}_{1.3}$

Table 2. Atomic percentage of Co, Fe, O and Mg in  $\text{Co}_{1-x}\text{Mg}_x\text{Fe}_2\text{O}_4$  ferrites.

Sample No.	$\text{Mg}^{2+}$ [mol] x	Co	Fe	O	Mg	Total
1	0.0	17.75	32.07	50.18	0	100
2	0.1	16.33	37.32	45.53	0.82	100
3	0.2	14.70	37.83	46.29	1.18	100
4	0.25	9.87	31.64	55.60	2.89	100

clear bands, characteristic of cubic spinels which correspond to the vibrations of the Th- and Oh-interstitial complexes. The strong absorption bands  $\nu_1$  ( $\sim 500 \text{ cm}^{-1}$  to  $650 \text{ cm}^{-1}$ ) and  $\nu_2$  ( $\sim 400 \text{ cm}^{-1}$  to  $490 \text{ cm}^{-1}$ ) observed in the FT-IR are assigned to the intrinsic stretching vibrations of metal oxygen bond at the tetrahedral site  $\text{M}_{\text{tet}}\text{-O}$  and to the stretching vibrations of metal oxygen bond at the octahedral sites  $\text{M}_{\text{oct}}\text{-O}$ , respectively [35]. Replacing  $\text{Co}^{2+}$  with non-magnetic  $\text{Mg}^{2+}$  ions at the octahedral sites and the resultant displacement of  $\text{Fe}^{3+}$  ions to tetrahedral sites result in the slight shifting of absorption band positions towards higher frequency. This shifts of frequencies  $\nu_1$  and  $\nu_2$  are due to the replacement of  $\text{Mg}^{2+}$ , which slightly influences the metal-oxygen force constants in the tetrahedral and octahedral sites. The bands at around  $1600 \text{ cm}^{-1}$  and  $2400 \text{ cm}^{-1}$  (Fig. 4) are assigned to the O-H stretching and H-O-H bending vibration modes of atmospheric water molecules (moisture content in the samples).

### 3.4. Raman spectroscopy

Raman spectra of  $\text{Co}_{1-x}\text{Mg}_x\text{Fe}_2\text{O}_4$  ( $x = 0.05$  to 0.25) samples annealed at  $1100 \text{ }^\circ\text{C}$  for 2 h are shown in Fig. 5. The space group  $\text{O}_h^7$  ( $\text{Fd-3m}$ ) shows 39 normal modes exhibited by  $\text{CoFe}_2\text{O}_4$  with cubic partial inverse spinel structure represented as:

$$\Gamma = A_{1g} + E_g + F_{1g} + 3F_{2g} + A_{2u} + 2E_u + 4F_{1u} + 2F_{2u} \quad (1)$$

Out of these modes, five Raman active optical modes ( $A_{1g} + E_g + 3F_{2g}$ ) and four infrared active optical modes ( $4F_{1u}$ ) in  $\text{CoFe}_2\text{O}_4$  are observed [36]. Report from previous work [37] states that Raman mode at  $694 \text{ cm}^{-1}$  (high frequency) is considered to be the mode with  $A_{1g}$  symmetry, which is assigned to the tetrahedral-site. The peak at  $475 \text{ cm}^{-1}$  is assigned to the octahedral site mode.  $\text{Fe}^{3+}$  ions in tetrahedral sites move to octahedral sites while  $\text{Co}^{2+}$  ions at octahedral sites move to tetrahedral sites during cation migration

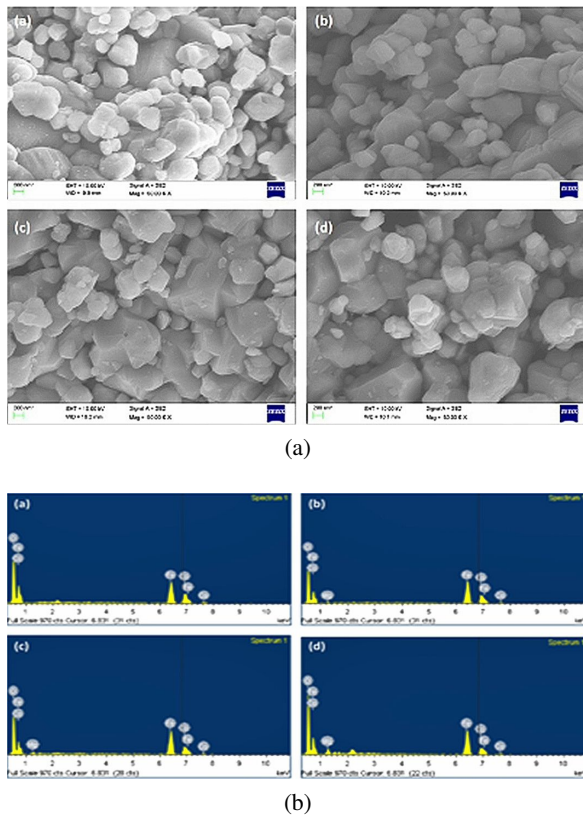


Fig. 3. (a) Scanning electron micrographs of  $\text{Co}_{1-x}\text{Mg}_x\text{Fe}_2\text{O}_4$  powder samples annealed at 1100 °C for 2 h; (b) EDX patterns of  $\text{Co}_{1-x}\text{Mg}_x\text{Fe}_2\text{O}_4$  powder samples annealed at 1100 °C for 2 h.

in  $\text{CoFe}_2\text{O}_4$ , which results in disorder between both sites [38]. The modes above 600 cm<sup>-1</sup> are usually assigned to tetrahedral ( $\text{AO}_4$ ) sites which are due to the stretching vibration of  $\text{Fe}^{3+}$  and  $\text{O}^{2-}$  ions in tetrahedral sites, while the other frequency modes are assigned to  $\text{E}_g$  modes reflecting the vibration of the octahedral site ( $\text{BO}_6$ ) in cubic spinels. The tetrahedral site is occupied by only  $\text{Fe}^{3+}$ , while the octahedral site is occupied by both  $\text{Co}^{2+}$  and  $\text{Fe}^{3+}$  ions. Due to the difference between ionic radii of  $\text{Co}^{2+}$  and  $\text{Fe}^{3+}$  present in  $\text{CoFe}_2\text{O}_4$ , redistribution of Fe–O and Co–O bonds between both the sites takes place. Due to this, broadening of Raman peaks is observed at  $\sim 205$  cm<sup>-1</sup>, 308 cm<sup>-1</sup>, 465 cm<sup>-1</sup> and 694 cm<sup>-1</sup>, respectively. At lower wave numbers, shifting of modes is observed owing to lower atomic mass of Mg as compared to Co [39]. The vibrational modes  $\nu_1$ ,  $\nu_2$ ,  $\nu_3$  and

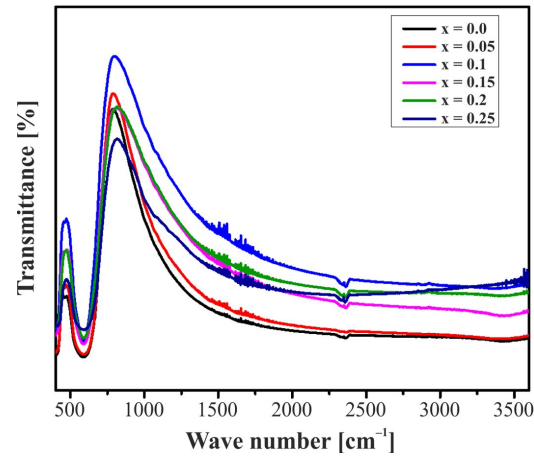


Fig. 4. FT-IR spectra of  $\text{Co}_{1-x}\text{Mg}_x\text{Fe}_2\text{O}_4$  powder samples annealed at 1100 °C for 2 h.

$\nu_4$  (Fig. 5) are attributed to the tetrahedral sites in which four modes correspond to Raman active, while two modes are IR active. The absence of strong modes at 407 cm<sup>-1</sup> in Raman spectra for the octahedral sites proves that either of the modes ( $\nu_3$  or  $\nu_4$ ) is strong in IR active region and weak in the Raman spectra [40].

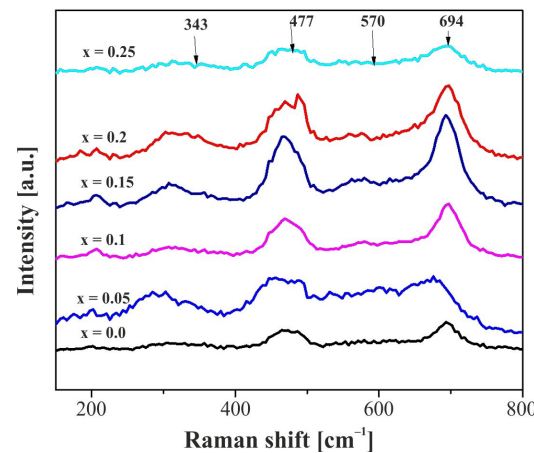


Fig. 5. Raman spectra of  $\text{Co}_{1-x}\text{Mg}_x\text{Fe}_2\text{O}_4$  powder samples annealed at 1100 °C for 2 h.

### 3.5. Magnetic properties

The magnetic properties of  $\text{Co}_{1-x}\text{Mg}_x\text{Fe}_2\text{O}_4$  ( $x = 0.05$  to 0.25) samples annealed at 1100 °C for 2 h, were characterized at room temperature using a vibrating sample magnetometer.

The M-H curves (Fig. 6a) were analyzed to extract magnetic information about the samples, such as the saturation magnetization ( $M_s$ ), remanence ( $M_r$ ) and coercivity ( $H_c$ ). The magnetization of a sample is decided by the interaction between (inter-sublattice) and amongst (intra-sublattice) magnetic moments present at the tetrahedral (A) and octahedral (B) sites. At room temperature, ferromagnetic behavior has been exhibited by all the samples and hysteresis loops were observed. The samples exhibit progressive magnetic softening with increasing Mg-content in the lattice. The high magnetic field ( $H = 15$  kOe) is insufficient to completely saturate Mg- substituted  $\text{CoFe}_2\text{O}_4$  samples resulting in steady linear increase in magnetization up to the applied field value of 15 kOe (Fig. 6a). In Table 3, the values of coercivity ( $H_c$ ) and saturation magnetization ( $M_s$ ) are provided. For our samples, variations of  $M_s$  in the range of  $149 \text{ emu}\cdot\text{g}^{-1}$  to  $228 \text{ emu}\cdot\text{g}^{-1}$  and  $H_c$  in the range of 563 Oe to 728 Oe are observed. Maximum  $M_s$  value of pristine sample is  $228 \text{ emu}\cdot\text{g}^{-1}$  and the obtained maximum  $M_s$  values of doped  $\text{Co}_{0.9}\text{Mg}_{0.1}\text{Fe}_2\text{O}_4$  and  $\text{Co}_{0.8}\text{Mg}_{0.2}\text{Fe}_2\text{O}_4$  samples are  $188 \text{ emu}\cdot\text{g}^{-1}$  and  $149 \text{ emu}\cdot\text{g}^{-1}$ , respectively. The decrement in  $M_s$  is caused by the presence of  $\alpha\text{-Fe}_2\text{O}_3$  impurity (Fig. 6). Due to the change in average atomic magnetic moment followed in Slater-Pauling curve [41], there is a rise in  $M_s$  of the samples (except  $\text{Co}_{0.8}\text{Mg}_{0.2}\text{Fe}_2\text{O}_4$ ) with an increase in Co/Fe [42] that takes place when the Co/Fe ratio is lower than 0.25. In compounds containing 3d transition metal atoms, the lattice parameters play a prominent role in deciding the magnetic interaction [43]. We notice that with an increase in magnesium concentration, there is a decrement in lattice parameter due to the smaller atomic radius of Mg (1.45 Å) compared to that of Co (1.52 Å).

### 3.6. Mössbauer spectroscopy

The Mössbauer spectra (Fig. 7) of all the samples show two clearly separated Zeeman split sextets indicating good magnetic order prevailing in spinel lattice. This is also evident from the low values of QS. All the IS values corresponding to A and B sites agree with the values for  $\text{Fe}^{3+}$  ions

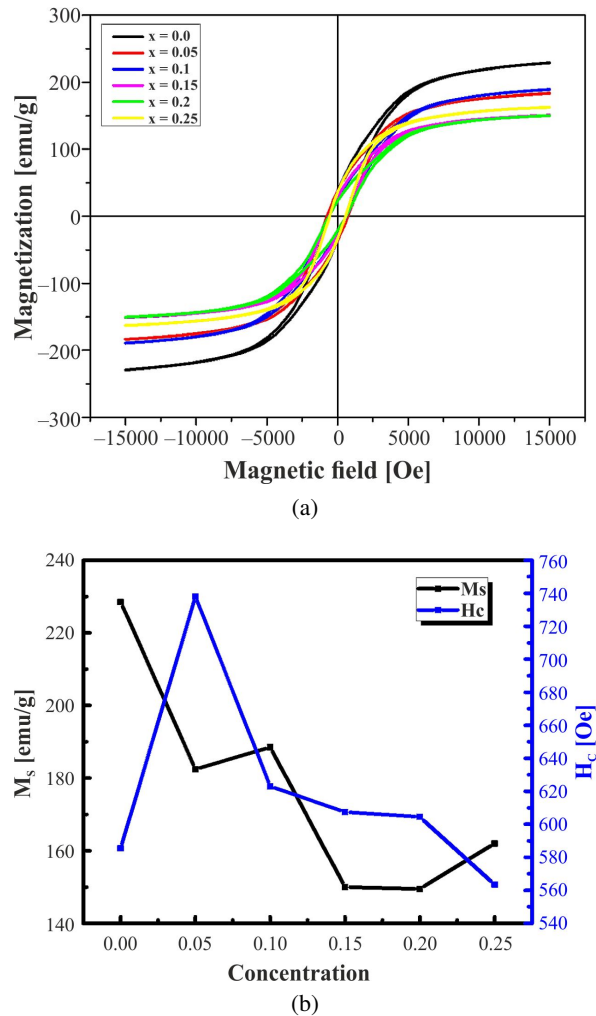


Fig. 6. (a) room temperature magnetic hysteresis loops of  $\text{Co}_{1-x}\text{Mg}_x\text{Fe}_2\text{O}_4$  powder samples annealed at  $1100^\circ\text{C}$  for 2 h; (b)  $M_s$  and  $H_c$  loops of  $\text{Co}_{1-x}\text{Mg}_x\text{Fe}_2\text{O}_4$  powder samples annealed at  $1100^\circ\text{C}$  for 2 h.

in these interstitials. Also, the magnetic hyperfine field ( $B_{hf}$ ) values for A- and B-sites are consistent with the  $\text{Fe}^{3+}$  at A- and B-sites [46]. The cation distribution analysis in the magnetic sub-lattices (i.e., A- and B-sites) for  $\text{CoFe}_2\text{O}_4$  sample shows the mixed spinel structure of the sample with occupancy of  $\sim 72\%$   $\text{Fe}^{3+}$  at B-site, while the rest of  $\text{Fe}^{3+}$  at A-site. This indicates a small fraction of  $\text{Co}^{2+}$  at the A-site, although  $\text{Co}^{2+}$  mainly occupies B-site. This result is in consistence with the Rietveld refinement results of XRD data (Table 1). Effect of Mg substitution is seen

Table 3. Saturation magnetization ( $M_s$ ), coercive field ( $H_c$ ), remanent magnetization ( $M_r$ ) and squareness ( $M_r/M_s$ ) of  $\text{Co}_{1-x}\text{Mg}_x\text{Fe}_2\text{O}_4$  ( $x = 0, 0.05$  to  $0.25$ ).

Chemical composition	$M_s$ [emu/g]	$H_c$ [Oe]	$M_r$ [emu/g]	$M_r/M_s$
CoFe <sub>2</sub> O <sub>4</sub>	228	585	34.6	0.15
Co <sub>0.95</sub> Mg <sub>0.05</sub> Fe <sub>2</sub> O <sub>4</sub>	182	738	36.5	0.20
Co <sub>0.9</sub> Mg <sub>0.1</sub> Fe <sub>2</sub> O <sub>4</sub>	188	623	24.76	0.13
Co <sub>0.85</sub> Mg <sub>0.15</sub> Fe <sub>2</sub> O <sub>4</sub>	150	607	27.50	0.18
Co <sub>0.8</sub> Mg <sub>0.2</sub> Fe <sub>2</sub> O <sub>4</sub>	149	604	22.35	0.15
Co <sub>0.75</sub> Mg <sub>0.25</sub> Fe <sub>2</sub> O <sub>4</sub>	162	563	34.61	0.21

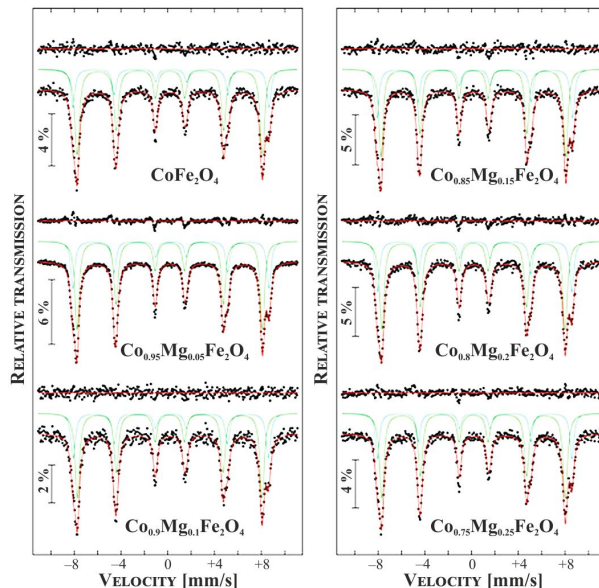


Fig. 7. Room temperature Mössbauer spectra of  $\text{Co}_{1-x}\text{Mg}_x\text{Fe}_2\text{O}_4$  powder samples annealed at  $1100^\circ\text{C}$  for 2 h.

as slightly reduced  $B_{hf}$  values, which progressively decrease with increasing substituent content (Table 4). This has been expected as the  $\text{Mg}^{2+}$  is non-magnetic, which magnetically dilutes the sub-lattices, reducing the super-exchange interaction. This is in accordance with the magnetization studies, where  $M_s$  values showed a decreasing trend with an increase in Mg content (Fig. 6). The ratio of crystalline sub-spectral area of A-site to B-site shows an increasing trend (Table 4) for Mg doped cobalt ferrite with the substituent concentration. This clearly indicates

the non-magnetic ions enter the A-sites preferably. Also, the  $\text{Co}^{2+}$  ions mostly occupy the B-site. This observation is also supported by the cation occupancies obtained from the Rietveld refinement of XRD data of the respective samples (Table 1), where the preferential occupancy of  $\text{Co}^{2+}$  at B-site resulted in major fraction of  $\text{Mg}^{2+}$  at the A-site. The hyperfine parameters IS and QS remained almost unchanged due to the preservation of crystal structure and low dopant concentration.

Although the sample  $\text{Co}_{0.8}\text{Mg}_{0.2}\text{Fe}_2\text{O}_4$  ( $\text{Co}_{1-x}\text{Mg}_x\text{Fe}_2\text{O}_4$  with  $x = 0.2$ ) showed the presence of hematite, the amount of this impurity phase is very small (Table 1). Also, since the sextet arising due to this phase overlaps with the contribution from A-site of the spinel ferrite, we have neglected hematite phase during the fitting procedure for the Mössbauer spectrum of  $\text{Co}_{0.8}\text{Mg}_{0.2}\text{Fe}_2\text{O}_4$  sample.

## 4. Conclusions

Polycrystalline Mg-substituted CoFe<sub>2</sub>O<sub>4</sub> samples were successfully synthesized by sol-gel method followed by thermal treatment. X-ray diffraction studies confirmed the formation of pure or near-pure phase samples (the intended phase was cubic spinel ferrite; space group Fd-3m), while a few samples showed trace amount of impurity phases. FT-IR spectroscopy supports the supposition that cations migrate between the octahedral and tetrahedral sites on Mg<sup>2+</sup> substitution. Raman spectroscopy confirms obtaining the products with cubic spinel structure. The cation distribution estimated from Mössbauer data are

Table 4. The Mössbauer spectral parameters for  $\text{Co}_{1-x}\text{Mg}_x\text{Fe}_2\text{O}_4$  with  $x = 0$ ,  $x = 0.05$ ,  $x = 0.1$ ,  $x = 0.15$ ,  $x = 0.2$ ,  $x = 0.25$ . The isomer shift (IS), quadrupole splitting (QS), magnetic hyperfine fields ( $B_{hf}$ ), line width, sub-spectral area.

Sample No.	Composition	Sub-spectra	Mössbauer hyperfine parameters				
			IS [mm/s]	QS [mm/s]	$B_{hf}$ [T]	Line-width [mm/s]	Sub-spectral area [%]
1	$\text{CoFe}_2\text{O}_4$	S1	0.278	-0.018	52.02	0.424	28.4
		S2	0.175	-0.019	49.16	0.470	71.6
2	$\text{Co}_{0.95}\text{Mg}_{0.05}\text{Fe}_2\text{O}_4$	S1	0.270	-0.012	52.04	0.419	33.7
		S2	0.165	-0.007	49.21	0.432	66.3
3	$\text{Co}_{0.9}\text{Mg}_{0.1}\text{Fe}_2\text{O}_4$	S1	0.266	-0.011	51.78	0.455	34.7
		S2	0.165	-0.007	49.0	0.448	65.3
4	$\text{Co}_{0.85}\text{Mg}_{0.15}\text{Fe}_2\text{O}_4$	S1	0.262	-0.001	51.87	0.425	35.4
		S2	0.159	-0.008	49.04	0.420	64.6
5	$\text{Co}_{0.8}\text{Mg}_{0.2}\text{Fe}_2\text{O}_4$	S1	0.264	0.002	51.51	0.420	33.2
		S2	0.161	-0.004	48.63	0.466	66.8
6	$\text{Co}_{0.75}\text{Mg}_{0.25}\text{Fe}_2\text{O}_4$	S1	0.272	-0.011	51.56	0.401	30.8
		S2	0.164	-0.007	48.69	0.459	69.2

in accordance with cation occupancies determined by Rietveld refinement of powder XRD data. Saturation magnetization increases initially and decreases with Mg content which is explained based on Slater-Pauling curve.

### Acknowledgements

The authors would like to thank Prof. Balan Guru Moorthy, Indian Institute of Science, Bangalore, for his help in carrying out the FT-IR measurements. Authors are also thankful to Dr. Balaram Sahoo for useful comments and suggestions.

### References

- [1] YI N., ALIVISATOS A.P., *Nature*, 437 (2005), 664.
- [2] GENG B.Y., MA J.Z., LIU X.W., DU Q.B., KONG M.G., ZHANG L.D., *J. Appl. Phys.*, 90 (2007), 043120.
- [3] SUN S., MURRAY C.B., WELLER D., FOLKS L., MOSER A., *Science*, 287 (2000), 1989.
- [4] JILES D.C., LO C.C.H., *Sensor. Actuat. A-Phys.*, 106 (2003), 3.
- [5] SLICK P.I., WOHLFRATH E.P. (ed.) in: *Ferromagnetic Materials*, Vol. 2, North-Holland, Amsterdam, 1980, 796.
- [6] ZAWRAH M.F., EL-OKR M.M., ASHERY A., ABOU HAMMAD A.B., *Middle E. J. Appl. Sci.*, 2077 (2016), 362.
- [7] RAJENDRAN M., PULLA R.C., BHATTACHARYA A.K., DAS D., CHINTALAPUDI S., NMAMJUMDAR C.K., *J. Magn. Magn. Mater.*, 232 (2001), 71.
- [8] LIU C., ZOU B., RONDINONE A.J., ZHANG Z.J., *J. Am. Chem. Soc.*, 122 (2000), 6263.
- [9] ZHANG Z.J., WANG Z.L., CHAKOUMAKOS B.C., YIN J.S., *J. Am. Chem. Soc.*, 120 (1998), 1800.
- [10] TEMPLETON T.L., ARROTT A.S., CURZON A.E., GEE M.A., LI X.Z., YOSHIDA Y., SCHURER P.J., LACOMBE J.L., *J. Appl. Phys.*, 73 (1993), 6728.
- [11] HANEDA K., MORRISH A., *J. Physique*, 38 (1977), C1-321.
- [12] HOSONO T., TAKAHASHI H., FIJITHA A., JOSEYPHUS J.R., TOHJI K., JEYADEVAN B., *J. Magn. Magn. Mater.*, 321 (2009), 3019.
- [13] BLASKOV V., PETKOV V.R., MARTINEZ L., MARTINEZ B., MONOS J., MIKHOV M., *J. Magn. Magn. Mater.*, 162 (1996), 331.
- [14] SRARAVANAN P., ALAM S., MATHUR G., *J. Mater. Sci. Lett.*, 22 (2003), 1283.
- [15] MAITY D., KALE S.N., KAUL-GHANEKUR R., XUE J.-M., JUN D., *J. Magn. Magn. Mater.*, 321 (2009), 3093.
- [16] HUA Z., CHEN R., LI C., YANG S., LU M., GU B., DU Y., *J. Alloy. Compd.*, 427 (2007), 199.
- [17] LIU M., IMRANE X.L.H., CHEN X.L.H., GOORICH T., CAI Z., ZEIMER K., HUANG J., SUN N., *Appl. Phys. Lett.*, 90 (2007), 152501.
- [18] SANTRA R., TAPE S., THEODOROPOULOUS N., DOBSON J., HEBARD A., TAN W., *Langmuir*, 17 (2001), 2900.
- [19] CHAE K.P., KIM W.K., LEE S.H., LEE Y.B., *J. Magn. Magn. Mater.*, 232 (2001), 133.
- [20] BAE C.Y., LEE K.P., LEE J.G., LEE S.H., *J. Magn. Magn. Mater.*, 220 (2000), 59.

- [21] YU T., SHEN Z.X., SHI Y., DING J., *J. Phys.-Condens. Mat.*, 14 (2002), 613.
- [22] DALIYA S.M., RUEY S.J., *J. Chem. Eng.*, 129 (2007), 51.
- [23] CORLISS L.M., HASTINGS J.M., *Phys. Rev.*, 90 (1953), 1013.
- [24] CHAE K.P., LEE J., KWEON H.S., LEE Y.B., *J. Magn. Magn. Mater.*, 283 (2004), 103.
- [25] SEPELAK V., MENZEL M., BECKER K.D., KRUMMICH F., *J. Phys. Chem. B*, 106 (2002), 6672.
- [26] HARRISON R.J., PUTNIS A., *Phys. Chem. Miner.*, 80 (1995), 213.
- [27] MITTAL V.K., SANTANU B., NITHYA R., SRINIVASAN M.P., VELMURUGAN S., NARASIMHAN S.V., *J. Nucl. Mater.*, 335 (2004), 302.
- [28] YOUNG R.A., *The Rietveld method*, IUCr, 15, Oxford University Press, Oxford, 1993, pp. 1 – 39.
- [29] RODRIGUEZ-CARVAJAL J., *FULLPROF – A Program for rietveld refinement and pattern matching analysis, abstracts of the satellite meeting on powder diffraction of the XV Congress of the IUCr*, Toulouse, 1990, 127.
- [30] WILLIAMSON W.H., HALL G.K., *Acta Metall.*, 1 (1953), 22.
- [31] GEORGE T., SUNNY A.T., VARGHESE T., *Mat. Sci. Eng.*, 73 (2015), 012050.
- [32] SHANNON R.D., *Acta Crystallogr. A*, 32 (1976), 751.
- [33] HORN VAN D.J., *Electronic Table of Shannon Ionic Radii*, on: <http://v.web.umkc.edu/vanhornj/shannonradii.htm>, accessed on: 2011.02.14.
- [34] FERREIRA T.A.S., WAERENBORGH J.C., MENDONCA M.H.R.M., NUNES F.M., COSTA M.R., *Solid State Sci.*, 5 (2003), 383.
- [35] SEZGIN N., SAHIN M., YALCIN A., KOSEOGLU Y., *Eko loji*, 22 (2013), 89.
- [36] AMMUNDSEN B., BURNS G.R., ISLAM M.S., KANO H., ROZIERE J., *J. Phys. Chem. B*, 103 (1999), 5175.
- [37] KREISEL J., LUCAZEAU G., VINCENT J., *J. Solid State Chem.*, 137 (1998), 127.
- [38] YU T., SHEN Z. X., SHI Y., DING J., *J. Phys.: Condens. Matter*, 14 (2002), 613.
- [39] VARSHNEY D., VARMA K., KUMAR A., *J. Mol. Struct.*, 1006 (2011), 447.
- [40] NAIK S.R., SALKER A.V., *J. Mater. Chem.*, 22 (2012), 2740.
- [41] WU A., YANG X.W., YANG H., *Dalton T.*, 42 (2013), 4978.
- [42] JILES D., *Introduction to Magnetism and Magnetic Materials*, Taylor & Francis, New York, 1998.
- [43] KOGACHI M., TADACHI N., ISHIBASHI H., *Intermetallics*, 13 (2005), 535.
- [44] BRAND R.A., *Nucl. Instrum. Meth. B*, 28 (1987), 398.
- [45] BRAND R.A., *Nucl. Instrum. Meth. B*, 28 (1987), 416.
- [46] KUNCSER V.V., SCHINTEIE G., SAHOO B., BICA K.W., VEKAS D., FILOTI G., *J. Phys.-Condens. Mat.*, 19 (2007), 016205.

Received 2017-06-05

Accepted 2018-03-28